Journal of Raman Spectroscopy

WILEY

Journal of RAMAN SPECTROSCOPY

RESEARCH ARTICLE OPEN ACCESS

The Complementary Use of Raman, ATR-FTIR Spectroscopy, and Chemometrics for Investigating the Deterioration of Artificially Aged Parchment

Ekaterini Malea[1] | Stamatis C. Boyatzis[1] | Dimitris Karlis[2] | Dimitrios Palles[3] | Soghomon Boghosian[4] | Spiros Zervos[5]

[1]Department of Conservation of Antiquities and Works of art, University of West Attica, Athens, Greece | [2]Department of Statistics, Athens University of Economics and Business, Athens, Greece | [3]Theoretical and Physical Chemistry Institute, National Hellenic Research Foundation, Athens, Greece | [4]Department of Chemical Engineering, University of Patras and FORTH/ICE-HT, Patras, Greece | [5]Department of Archival, Library and Information Studies, University of West Attica, Athens, Greece

Correspondence: Ekaterini Malea (kmalea@uniwa.gr)

Received: 5 February 2024 | **Revised:** 8 November 2024 | **Accepted:** 11 November 2024

Keywords: aged parchment | ATR-FTIR | chemometrics | parchment degradation | Raman

ABSTRACT

Among the materials constituting our cultural heritage, parchment has a significant role as the substrate of many archival documents. The assessment of its state of preservation has an important benefit to conservation and delineates the adequate preventive measures that would lead to better-controlled storage and exhibition conditions in museums and libraries worldwide. In the framework of this project, artificial aging of 48 new goat parchment samples was performed to induce deterioration similar to naturally aged parchment exposed to atmospheric pollutants. Five factors have been examined: relative humidity; NO_2; SO_2; exposure time, and the order of sequential exposure to NO_2 and SO_2. Temperature was kept constant at 25°C, while the effect of the above-mentioned factors was examined at two levels (low and high). Statistics was involved in advance in the experimental design. Raman spectroscopy along with attenuated total reflectance-Fourier transform infrared (ATR-FTIR) spectroscopy were used to investigate the condition of collagen in parchment. The entire set of environmental factors along with detected changes in the spectra were investigated through a chemometrics scheme involving analysis of variance (ANOVA). According to the results, the onset of collagen's secondary structure decomposition was observed. Statistical elaboration of data reveals that the two analytical methods (Raman and ATR-FTIR) function in a complementary manner related to the molecular changes and the chemical reactions that happen. In conclusion, both methods can increase their impact on the investigation of parchment degradation if they are combined with other analytical methods and chemometric applications.

1 | Introduction

Archives and libraries are important repositories of memory, providing reliable evidence for examining the past and embodying an important set of social and cultural values of the world's heritage.

Archival material can cover a very broad spectrum ranging from classical documents to cartographic products. In addition to paper, papyrus, and leather, parchment is the substrate for many valuable documents and historical manuscripts [1]. Organic materials, including these substrates, can be affected by various environmental factors and are therefore vulnerable to damage. Ensuring the sustainability and resilience of collections is a shared objective worldwide. The preservation of these cultural artifacts is, therefore, a main concern of conservators and conservation scientists worldwide.

To achieve the goal of preservation, it is first and foremost necessary to understand the mechanisms of deterioration of the material. For this reason, within Europe, research on the effects of air pollutants, temperature, relative humidity, light, and microorganisms on the degradation of organic materials constituting cultural heritage has been carried out for decades in specialized museums, universities, research institutes, and by environmental agencies, which managed to establish several collaboration projects at the European level (IDAP, AER, IMPACT, LIDO, MIMIC, MASTER, MIP, ERA, SENSORGAN, PAPYLUM, SURVENIR, INKCOR, PAPERTREAT, PARELA, CARAMEL, MULTIENCODE, VIDRIO, MODHT, PROPAINT, and MEMORI) [2].

Most relevant research projects have used artificial aging methods to simulate the mechanisms of natural aging and to determine the effects on these documents after long-term exposure to environmental factors. The aging protocols followed include specific deterioration factors (SO_2, NO_2, Relative Humidity, Temperature, UV/VIS Light) but vary in combinations of these, duration of exposure, and intensity levels [3–13].

A common point in most of these research processes is the use of relatively harsh aging protocols as a starting point to obtain significant results that a milder variant might not have provided. [11]

The main objective of this research is to examine the impact of mild environmental conditions on the structural and material integrity of artificially aged parchment samples based on a statistically optimal experimental design. To achieve this, attenuated total reflectance-Fourier transform infrared (ATR-FTIR) and Raman analyses were used along with statistical processing of diagnostic data. Moreover, the two analytical methods are evaluated in terms of the complementarity they may have in maximizing the information they provide concerning the research questions posed.

2 | Background

2.1 | Parchment Composition and Morphology

Parchment is made from animal skin, and the production of parchment has followed the same basic procedure since ancient times. After the skin has been removed from the animal and has been washed, the hairs are loosened using a lime bath ($Ca(OH)_2$) and removed physically by scraping. The dehaired skin is mounted on a frame, dried under tension, and scraped with sharp knives until the desired thickness is obtained [14, 15]. While stretched on the frame, the collagen fibers within the skin are coaligned, basically resulting in a lamellar structure [16].

The skin can be divided into three main layers, where the outer layer is the epidermis, next is the dermis consisting of the grain and the corium layers. The hypodermis is below the dermis layer. In the two-dimensional structure, it can be difficult to detect the borderline between the grain and corium layer. Removal of the epidermis and hypodermis during the scraping process will leave only the dermis layer. If the parchment is produced for writing purposes, the grain is at least partly removed; and the surface may be rubbed with pumice stone.

In general, collagen molecules are built of repeating sequences of the amino acid glycine (Gly)-X-Y, where the X and Y positions are often taken by proline (Pro), hydroxyproline (Hyp), and alanine (Ala). Collagen I is a helix of two α1[I] and one α2[I] peptide chains. Collagen III is a helix of three α1 [III] peptide chains. The α1 chains in Collagen I and III are not identical but differ in their amino acid distribution and their chain length [17]. Each helical chain consists of more than 1000 amino acids. Apart from the presence of cysteine (Cys), Collagen III is characterized by a lower content of Ala and aspartic acid (Asp) and also higher content of asparagine (Asn), serine (Ser), and histidine (His), compared to Collagen I [18].

During the liming process, some of the Asn and glutamine (Gln) residues are transformed into Asp and glutamic acid (Glu) by deamidation. Furthermore, some arginine (Arg) residues are hydrolyzed into ornithine (Orn) under the release of urea [14]. As Asp and Glu as well as Arg are present in both Collagens I and III, these modifications must take place in both collagen types.

Collagen fibers can be considered as robe-like structures [19] made from twisted bundles of the smaller collagen fibrils; these again are twisted from collagen molecules consisting of three peptide chains coiled together in a triple helix. Each peptide chain is a left-handed helix, when coiled together results in the right-handed collagen molecule and so forth left and right [14]. The length of the collagen molecule is around 300 nm.

The structural composition and chemical properties of the parchment are closely linked. All mammals have the following skin characteristics, which are thereby also visible on parchment: specific pattern of hair follicles, the diameter of collagen fibres, spatial placement of helixes, the thickness of the skin, different structures, and thickness of the three skin layers. These characteristics determine the physical and chemical properties of the skin and can vary among animal species or individuals of the same species (due to genetic and epigenetic factors). Structure variations also exist with location in the skin due to the biodiversification of the animals' integumentary system [20].

2.2 | Factors Affecting the Aging Process of Parchment and the Consequence Hereof

Generally, parchment is a relatively stable and long-lasting material. However, long periods of subjection to either high relative humidity (RH), air pollutants, microorganisms, high temperatures, or too much sunlight (or a mixture of these) will inevitably lead to degradation. Parchment is highly hygroscopic, and changes in RH and temperature quickly lead to dimensional changes (i.e., thickness) of the parchment. The chemical deterioration of parchment causes the collagen to denaturize. This is detectable as a characteristic morphological transformation, which may lead to a complete gelatinization of the collagen [6].

2.3 | Methods for the Evaluation of Parchment Properties

Parchment is composed mostly of the protein collagen, which displays a discrete structural hierarchy, from the molecular to microscopic levels. Collagen degradation at any or all levels of the structural hierarchy over time may influence the physical characteristics of historically important documents. Moreover, the damage picture may change from one structural level to another [6].

It has been shown that the progress of damage from outside to inside may take place on all structural levels from the macroscopic to the molecular; that is, some assessment methods like visual evaluation, fiber assessment, thermochemical and thermophysical techniques, and X-ray diffraction (XRD) measure the summarized total effect of deterioration on the parchment structure, whereas other methods like amino acid analysis and FT-Raman are more specific in the detection of oxidative and hydrolytic breakdown, respectively [6].

At the macroscopic level, changes to characteristics like color, stiffness, thickness, and transmission of light may reflect damage and are measurable by simple techniques. At the microscopic level, damage in the fiber structure is detectable and measurable by light microscopy and hydrothermal stability by the microhot table technique (MHT). However, deterioration is not always visually detectable, and this may lead to further damage of the parchment caused by inappropriate treatment or storage conditions. Therefore, systematic detection of all relevant characteristics detected by simple and visual methods, which may indicate damage and material breakdown processes, is the most effective way to get better information on the condition of the parchment as a basis for its treatment and future protection in storage and on exhibition. Moreover, analysis of the assessment data including its correlation to data from advanced analysis and experiments will add knowledge and experience of the characteristics and evolution patterns of deterioration and the causes thereof [6].

Furthermore, damage in the parchment on the mesoscopic and nanoscopic levels is detectable by analytical techniques such as scanning electron microscopy (SEM), transmission electron microscopy (TEM), differential scanning calorimetry (DSC), and atomic force microscopy (AFM), respectively. On the molecular level, techniques like Fourier transform (FT)-Raman, Fourier transform infrared (FTIR) spectroscopy, gas chromatography–mass spectrometry (GC–MS), high-performance liquid chromatography (HPLC), nuclear magnetic resonance (NMR) spectroscopy, solid-phase microextraction followed by gas chromatography–mass spectrometry (SPME–GC/MS), and XRD can be used [3]. Moreover, the mechanical, thermochemical, and thermophysical behaviors can be measured using techniques such as DSC, dynamic mechanical thermal analysis (DMA), and thermogravimetry (TGA).

Vibrational spectroscopy, such as infrared and Raman, can provide information on the chemical bonding of the material [21, 22]. Both techniques have been extremely useful in evaluating protein-based materials such as skin and parchment in the fields of health sciences [23] as well as cultural heritage [24, 25]. Both techniques offer a panoramic view of bonding in collagen as the main material, lipids originally existing in the animal tissue, as well as calcium carbonate as the end product due to the liming process in the manufacture of parchment.

2.3.1 | Raman Spectroscopy

Micro-Raman spectroscopy has been used in the study of proteins, especially in the field of health sciences, where it forms part of the study of human cells, including lipids and DNA/RNA as well. The technique has proved particularly useful in cases where a spatial resolution better than 1 μm is required to study variations of the protein structure; several variants of Raman spectroscopy, either more traditional like surface-enhanced Raman scattering (SERS), tip-enhanced Raman spectroscopy (TERS), coherent anti-Stokes Raman scattering spectroscopy (CARS), or novel like transmission or spatially offset Raman, have also been applied—see, for example, [26] and references therein. Relatively fewer studies have focused on protein materials in cultural heritage [5, 27, 28]. Despite the fact that this technique also offers information on molecular bonding as a result of the molecular vibrations, it is often considered a complementary technique to FTIR, based on the different phenomena and principles they are based on, absorption of infrared radiation for FTIR, and inelastic scattering of usually visible or near infrared (NIR) radiation for Raman. Since in most cases, the protein structure is noncentrosymmetric, most vibrational modes are both infrared and Raman active, albeit with some wavenumber differences as observed by the two techniques.

2.3.2 | ATR-FTIR

ATR-FTIR has possibly been the most widely applied technique for noninvasively investigating parchment on a molecular level. Utilizing a high refractive index crystal (in our case diamond) in close contact with the sample surface takes advantage of the total internal reflection phenomenon, where an evanescent infrared wave penetrates the sample by 1–3 μm [29, 30]. The absorbed radiation provides chemical information about the bonding in molecules. This technique is possibly the most widely used for soft materials such as parchment and leather. There has been a wealth of data published on infrared spectroscopy of these specific protein materials [31–35]; protein infrared spectra have characteristically broad bands, with their maxima reflecting the vibrations of the various molecular bonds, while their envelope reflects intermolecular interactions such as hydrogen bonding [36–40].

2.3.3 | Statistical Analysis and Chemometrics

Chemometrics is the application of mathematical and statistical methods in chemistry. It involves designing or selecting experimental plans and procedures for physical–chemical analysis to extract maximum information through algorithmic processing of data obtained from laboratory or industrial studies. In cultural objects' degradation studies, the method relies on analyzing data from collections of existing objects using advanced statistical techniques to identify factors that may be responsible for the

deterioration of these objects and determine the key factor that can contribute to their preservation [41–49]. It is generally used in situations where theoretical knowledge of physical–chemical processes and states is insufficient to describe or solve problems in the study of these systems. The main objective of chemometric techniques is to highlight complex and nonobvious relationships between a large number of variables associated with the studied systems, using statistical–mathematical models capable of describing states of physical–chemical systems at a given time or in their dynamic.

Statistical analysis has been used in the elaboration of data in the conservation sciences field, though not based on a statistical design, to determine the deterioration factors affecting parchment and/or to estimate its state of preservation. For example, statistical methods were applied to uncover the pattern behind the deterioration of parchments [7], while a recent publication [5] presented the application of factorial analysis of mixed data (FAMD) to explore the correlation between aging conditions and spectroscopic variables and identify spectroscopic features for different aging conditions.

2.4 | Aims of This Work

The research aims to determine the degree of parchment degradation after artificial aging and to correlate the degradation patterns with the environmental factors to which it was exposed. To achieve this objective, a protocol of exposing the samples to mild aging conditions (low concentration of air pollutants, constant temperature of 25°C, and no extreme RH values) was applied to identify, via statistical processing of the data, the factors that trigger the degradation processes. Analytical methods (such as ATR-FTIR and Raman) that provide information on the preservation status of parchment at the molecular level were selected to evaluate their accuracy and the added research value achieved by their combination.

3 | Experimental

3.1 | Samples

According to similar studies [11], it was decided to use only one type of parchment rather than various different samples, to obtain a "model set". This was in order to observe the effects of different aging parameters rather than the varied reactions of different parchment materials, which would have been difficult to distinguish from environmental influences.

The parchment hide used in this study has been acquired by the National Research and Development Institute for Textile and Leather (I.N.C.D.T.P.), Bucharest Romania. The material has been produced by traditional methods and it was chosen for this purpose because it is similar to historical materials met in collections and museums. The preparation protocol includes preservation of the skin by salting. The first stage of skin processing, soaking, is done with clean water of about 22°C. After soaking and fleshing, the liming operation is performed, 6%–8% Ca $(OH)_2$, whose main objective is the removal of the epidermis and hair. The skin is treated with a solution of lime for 3–4 days. The mechanical or manual fleshing is done before the second liming operation of about 2–3 days, 3%–4% Ca $(OH)_2$. Then, deliming and washing operations are performed and at the end the skin is stretched over a wooden frame and left to dry.

In this study, 96 samples have been analyzed in total. For the experimental process, 48 samples randomly chosen from a goat parchment hide have been used (Figure S1). They have been cut in the middle so 48 of them have been subjected to artificial aging with the protocol described here above, while the rest 48 remained as reference samples. This happened because parchment's characteristics and properties may vary a lot in the same hide topography. Thus, it was necessary to have a reference sample for each artificially aged sample, not from a near location but from the exactly adjacent place. For each cycle of artificial aging, three rectangular samples of 2 cm × 6 cm size have been used in order to have enough material for statistically safe results.

3.2 | Experimental Design

Experimental design refers to the process of carrying out research in an objective and controlled fashion so that precision is maximized, and specific conclusions can be drawn regarding a hypothesis statement. On the other hand, a proper design can reduce the cost of the experiment while at the same time producing sufficient information to test the scientific hypotheses of interest. As such, it can improve a lot our knowledge and ability towards scientific discoveries.

It is common that experiments involve the study of the effects of multiple factors. For such studies, the factorial experimental design is very useful. A full factorial design, also known as fully crossed design, refers to an experimental design that consists of two or more factors, with each factor having multiple discrete possible values or "levels". Using this design, all the possible combinations of factor levels can be investigated in each replication. Although several factors can affect the variable being studied in factorial experiments, this design specifically aims to identify the main effects and the interaction effects among the different factors. In a factorial design, each level of one independent variable is combined with each level of the others to produce all possible combinations. Each combination, then, becomes a condition in the experiment. A full factorial design with five factors with two levels each implies 32 replications.

Since aging can be a time-consuming procedure, recall that duration was itself a factor, this can increase the effort and cost of the experiment. In order to create a proper experimental design so as to make the investigation of the problem at hand feasible and taking into account time and cost restrictions, we have created a fractional factorial design based on the five above factors, assuming two levels for each factor.

Fractional factorial designs are experimental designs consisting of a carefully chosen subset (fraction) of the experimental runs of a full factorial design. The subset is chosen so as to exploit the sparsity-of-effects principle to expose information about the most important features of the problem studied, while

using a fraction of the effort of a full factorial design in terms of experimental runs and resources. In other words, it makes use of the fact that many experiments in full factorial design are often redundant, giving little or no new information about the system. The design of fractional factorial experiments must be deliberate, as certain effects are confounded and cannot be separated from others. In our case, we ended with a fractional factorial design with 16 replications (instead of 32 for the full factorial). Table 1 presents the experimental setup for the 16 replications used.

3.3 | Artificial Aging

Accelerated aging of new goat parchment samples was performed to induce artificial deterioration similar to naturally aged parchment exposed to atmospheric pollutants. Four factors affecting the aging process have been examined, namely, (i) relative humidity, (ii) the effect of NO_2, (iii) the effect of SO_2, and (iv) exposure time. Additionally, a fifth factor pertaining to the order of exposure to NO_2 and SO_2 has also been examined. Temperature was kept constant at 25°C, while the effect of the above four mentioned factors was examined at two levels (low, high). Hence, relative humidity was examined at levels of 45% and 70% as these are the lower and upper limits recommended for the storage and display of parchments [50]. Although the optimal value lies at a stable point between 45% and 60% relative humidity, the limits set for the current experiment are the extreme where either cracking and distortion or biological growth can happen respectively beyond these values. The gaseous pollutant concentrations were examined at levels of 10 and 25 ppm. The presence of these gaseous pollutants (NO_2 and SO_2) in industrial and urban areas does not exceed 0.5 ppm. Kobayashi and Yoshizumi [51] have calculated the urban concentration to achieve accelerated aging relevant to many years of exposure. Therefore, 10 ppm corresponds to nearly 20 times the exposure of an urban environment, while 25 ppm corresponds to 50 times. Finally, two durations of the experiments were chosen: one short duration (14 days) and one long (28 days).

The flow diagram of the aging chambers is shown in Figure S2. The gas mixing unit had four Brooks (Model 5850) mass flow controllers. The gasses used were 100 ppm SO_2/N_2 (Linde), 100 ppm NO_2/N_2 (Linde), and synthetic air (Linde). The pollutant streams (one at a time) and a dry stream of air were fed directly to a mixing point, where an additional stream of air saturated with humidity was also fed and hence the formulated mixture of a pollutant (NO_2 or SO_2) and humid air was fed to the aging chambers containing the parchment samples. The level of relative humidity was adjusted by mixing the dry and humidity-saturated streams at suitable relative flow rates. "Wetting" of the humidity-saturated air stream was achieved by bubbling dry air to saturation through water which was contained in two flasks connected in series and immersed in a thermostat controlled at the appropriate temperature (see Figure S2). Total flow rates in the range of 30 to 45 cm^3/min were used. In order to avoid condensation of water inside the tube network, all tubing (stainless

TABLE 1 | Fractional factorial design used for the experiments and the combinations of the five factors.

	Factors				
No of experiment	**RH**	**SO_2**	**NO_2**	**Duration**	**Order[a]**
1	45%	25 ppm	10 ppm	14 days	N/S
2	70%	10 ppm	25 ppm	28 days	N/S
3	70%	25 ppm	10 ppm	28 days	N/S
4	70%	10 ppm	10 ppm	28 days	S/N
5	45%	25 ppm	25 ppm	14 days	N/S
6	70%	10 ppm	25 ppm	28 days	S/N
7	70%	10 ppm	10 ppm	14 days	N/S
8	45%	25 ppm	25 ppm	28 days	N/S
9	45%	25 ppm	10 ppm	28 days	S/N
10	70%	25 ppm	25 ppm	28 days	S/N
11	45%	10 ppm	10 ppm	28 days	N/S
12	45%	10 ppm	25 ppm	14 days	N/S
13	70%	25 ppm	10 ppm	14 days	S/N
14	45%	25 ppm	25 ppm	14 days	S/N
15	45%	10 ppm	10 ppm	14 days	S/N
16	70%	10 ppm	25 ppm	14 days	S/N

[a]N/S and S/N denote the sequence of applying NO_2 (N) and SO_2 (S), for example, N/S means that treatment with NO_2 precedes the treatment with SO_2.

steel or borosilicate glass) was heated by electric resistances and heating tapes.

3.4 | Instrumentation

3.4.1 | Raman Spectroscopy

The Raman spectra have been acquired in the backscattering geometry using a dispersion micro-Raman photometer, employing an exciting solid state laser line at 785 nm. The laser beam on the sample has a quasi-rectangular shape of ~20×4 μm when the microscope is used with the ×50 objective lens (N.A. 0.75). The use of a lower magnification lens (×5, beam size ~200×40 μm or ×20) would yield a more representative spectrum, but as the Raman signal was weaker and the relative photoluminescence was higher, it was not chosen. The sampling penetration depth is generally larger than the one for the ATR technique and is estimated to be ~ 10 μm.

To reduce the parasitic luminescence signal, we used the photobleaching option of the spectrometer: It was experimentally determined that an exposure time of 210 s (right before spectral acquisition, using the same laser power of ~ 25 mW) gave the lowest possible luminescence signal. Thus, Raman spectra of all the samples were acquired with the 785-nm line using this photobleaching exposure time, in the 1800–100 cm^{-1} region. For reproducibility, spectra were recorded on three spots of both grain and flesh faces in each sample.

The micro-Raman photometer used was a Renishaw inVia Reflex system equipped with a metallurgical microscope and Peltier-cooled CCD camera. The manufacturer spectral resolution for the combination of the laser line and grating (1200 grooves/mm) is ~ 1 cm^{-1}, but since the Raman spectra digitization spacing is ~ 1 cm^{-1}, for complete correspondence with the infrared spectra, we can consider the Raman spectra resolution to be ~ 2 cm^{-1} (i.e., two times the digitization spacing).

Since intensities in all Spectra greatly varied, they were normalized on the amide I at ~1668 cm^{-1} by means of Spectragryph v.1.2.15 software. Baseline correction followed by applying the "adaptive" option at 20% coarseness, of "Advanced Baseline Routine" routine in SpectraGryph, which minimally affected the relative band intensities in all spectra. This is assumed to be the least variable band, since the carbonyl bond, its main contributor, is expected to be the least affected during the selected aging processes.

3.4.2 | Infrared Spectroscopy

FTIR was conducted employing a Bruker Alpha II Infrared Spectrometer in ATR mode with a Bruker single-reflection ATR accessory with diamond crystal as the internal reflection element. Parchment samples were placed on the ATR crystal and were accordingly pressed gently; for reproducibility, spectra were recorded on three spots of both grain and flesh sides in each sample. All spectra were recorded at 4000–400 cm^{-1} with 4 cm^{-1} resolution and were consequently processed with the Bruker Opus v. 8.5 software and consequently with the SpectraGryph v.1.2.15 software, through which the final spectrum images were produced.

Since spectra were recorded in variable intensities, they were normalized on the least variable band (see above similar for Raman spectra), amide I at ~ 1640 cm^{-1}. Baseline correction followed by applying the "adaptive" option at 30% coarseness, of "Advanced Baseline Routine" routine in SpectraGryph, which minimally affected the relative band heights in all spectra.

3.5 | Data Elaboration and Statistical Analysis

Certain Raman and FTIR spectrum observables, such as band maxima, their intensities, and their envelope characteristics, were selected and accordingly fed into the ANOVA model. More particularly, Raman bands maxima and intensities at 305, 531, 570, 622, 1002, 1028, 1245, and 1670 cm^{-1} were examined. Similarly, FTIR bands of parchment at 1640 cm^{-1} (amide I) and 1550 cm-1 (amide II) were considered, in both their broad-band form in the original spectra and their second derivative form, as negative, sharp peaks corresponding to the inflection points of the band envelopes. Additionally, the lipid carbonyl band at 1739 cm^{-1}, the amide III band at 1230 cm^{-1}, as well as that of calcium carbonate asymmetric stretch at 1410 cm^{-1} were considered for data elaboration.

The initial data used were the full curves taken from the spectroscopic analysis. Some initial examination revealed minor issues with the data, like negative values that have been corrected. Each sample was associated with the experimental conditions as well as the position of the parchment hide. We have also tested whether the position of the sample in the hide could have an effect on the results. In total, 581 observations were taken from FTIR and 216 from Raman. We denote the i-th spectrum as $Y_i^{(a)}$ where the superscript denotes the type of spectrometry, $a \in \{F, R\}$ where F implies FTIR and R Raman. This vector contains the entire range of measurements, and hence, $Y_i^{(a)} = \left(Y_{1i}^{(a)}, \ldots, Y_{Ni}^{(a)}\right)$ denotes the N measurements that fully define the spectrum of the i-th observation of the method α. In our case, we have measured the spectra in the 400–4000 cm^{-1} (~1800 cm^{-1}) and 100–1800 cm^{-1} (1769 cm^{-1}) ranges for FTIR and Raman, respectively.

Each observation is also associated with a certain number of characteristics (position of band maximum, intensity, and envelope) that refer to the experimental conditions (five factors), whether it is REF or AGED, the position of the sample in the parchment, and whether it was in the flesh or the grain side of the parchment. Based on the each spectrum observation $Y_i^{(a)}$ we can derive a series of measurement data denoted as $f_m\left(Y_i^{(a)}\right)$; these can be the band intensities at particular wavenumber that have some chemical interpretation and we wish to investigate whether they support certain hypotheses or even the entire area under the spectrum (integral) to be able to test hypotheses about the entire curves. These quantities will be used later in the analysis.

For each quantity of interest $f_m\left(Y_i^{(a)}\right)$, we have applied a typical analysis of variance (ANOVA) hypothesis testing. Namely, we have applied a linear model with response variable the quantity of interest and as explanatory variables the five factors of the experiment, while correcting for the baseline measurement in the reference sample from this parchment sample, that is, the relevant value of the REFERENCE group. Also, the side of the parchment was used to control for any differences. In order to account for the fact that we run multiple hypothesis testing, we have applied Bonferroni correction for multiple testing [52–54]. If multiple hypotheses are tested, the probability of incorrectly rejecting a null hypothesis (i.e., making a Type I error) increases. The Bonferroni correction compensates for that increase by testing each individual hypothesis at a significance level of α/m, where α is the desired overall alpha level and m is the number of hypotheses. In our case, m is the number of modes tested (9 for Raman and 3 for FTIR).

4 | Results and Discussion

4.1 | Raman Results

All samples resulted in the typical protein profile showing the amide I and III bands and the additional bands discussed in Section 2.3.1. Calcium carbonate in the form of calcite is observed at variable amounts (bands at ~ 152, 281, 712–3 and 1085–6 cm^{-1}) [55], as the result of liming through the manufacturing process; the grain side appears generally richer, in agreement with the ATR-FTIR measurements (see below). Raman spectra of collagen-based materials result in a multitude of peaks including the so-called amide I (1700–1600 cm^{-1}) and amide III (1425–1150 cm^{-1}) spectral regions, reflecting similar bonding to those in FTIR (the amide II band is practically inactive in Raman). Moreover, C–H (e.g., CH_2, CH_3 bend in the region 1480–1410 cm^{-1}) and C–C bonding (various skeletal C–C stretches in the region 1130–1060 cm^{-1} and aromatic ring and other C–C stretches in the region 1005–600 cm^{-1}) can be observed [5, 27, 28]. To these, the additional observation of C–S bonding (methionine and cysteine/cystine residues in the region 630–590 cm^{-1}) and S–S bonding (cystine residues in the region 580–500 cm^{-1}) grants an advantage, the latter being useful for monitoring the condition of collagen [5]. Spectra are shown in Figure 1, while band maxima and assignments are listed in Table 2. Of particular interest, even though not so strong in intensity, are the C–S bonding (methionine and cysteine/cystine residues in the region 630–590 cm^{-1}) and S–S bonding (cystine residues in the region 580–500 cm^{-1}) vibrations, the latter being a useful tracker of the collagen condition.

Specifically, cysteine exists in relatively high amounts in collagen propeptides which are involved in the extracellular construction of collagen in tissues such as skin and cartilage [57].

Cysteine, in the form of cystine (its dimer), is crucial in collagen's secondary and tertiary structure (i.e., the triple helix formation); although most of this amino acid is removed post-secretion, residual cysteine/cystine can be expected in certain collagen types, such as type III [58, 59].

Two new bands appear in the aged samples at ~ 1014 and 1045 cm^{-1}: these are assigned to the symmetric stretch vibrations (ν_1) of sulfate (SO_4) and nitrate (NO_3) salts, respectively, formed most probably with Ca as the charge balancing cation, being present as a result of the liming. The value of the 1014 cm^{-1} band points to the formation of bassanite ($CaSO_4 \cdot 0.5H_2O$), which is a mineral polymorph not as stable as gypsum or anhydrite I or II but neither metastable as anhydrite III [60]. The value of the 1045 cm^{-1} band points to the formation of a hydrated nitrate, since the cubic anhydrous Ca $(NO_3)_2$ shows its ν_1 band at ~ 1070 cm^{-1} [61] and the Ca $(NO_3)_2 \cdot 4H_2O$ hydrated salt shows a ν_1 band at ~ 1052 cm^{-1} [62].

Thus, in Figure 1, spectra appear this way, where intensity changes in all other peaks can clearly be seen, in both sides (grain and flesh), for aged and reference samples.

4.2 | ATR-FTIR Results

All samples resulted in the typical protein profile showing the amide I, II, and III bands and the additional bands discussed in Section 2.3.2. In addition, lipids are observed, mainly in the grain side through their carbonyl stretch at 1739 cm^{-1} and their C–H stretching absorptions at 2920 and 2852 cm^{-1}. Also, calcium carbonate is observed at variable amounts, as the result of liming through the manufacturing process; grain side appears generally richer. Thus, a typical pattern is detected including (a) the broadly shaped amide A and B (3300–3100 and 3080–3050 cm^{-1}, respectively) due to Fermi resonance of N–H stretch and amide II overtone [40, 63], (b) amide I (1660–1620 cm^{-1}) due to carbonyl stretch, with C–N stretch and N–H bend, (c) amide II (1570–1520 cm^{-1}) due to C–N stretch coupled with N–H bend, and (d) amide III (1240–1230, 1203 cm^{-1}) due to contributions by C–N stretch, N–H bend, C–C stretch, and C=O in-plane bending [34, 36, 40, 64–66]. In addition, the CH_2 stretching and bending due to glycine and proline moieties is observed at 2920, 2852, and 1445 cm^1. The medium-weak bands at 1080 and 1033 cm^{-1} are possibly due to H–C–C in-plane bending or the ring vibration of proline [67]. Spectra are shown in Figure 2, while band maxima and assignments are listed in Table 3. Thus, in Figures 2, S3, and S4, spectra appear this way, where intensity changes in all other peaks can clearly be seen.

The distance between amide I and amide II $\Delta\nu$ (A_I-A_{II}) is perceived as a marker for protein deterioration [35, 71], in reference spectra of grain side, where the carbonate content is generally excessively high, the amide I band maximum is located at 1650, and amide II at 1540 cm^{-1}, with a $\Delta\nu$ (A_I-A_{II}) of 110 cm^{-1}. This stays unchanged in aged spectra of the same parchment side, suggesting no detectable deterioration effect. On the other hand, in the reference spectra of flesh side, (typically, of low carbonate content), amide I appears at 1644 cm^{-1}, amide II at 1538 cm^{-1}, with a $\Delta\nu$ (A_I-A_{II}) distance of 106 cm^{-1}, similar to that of grain side. These values shift to 1633 and 1545 cm^{-1}, respectively, with a $\Delta\nu$ (A_I-A_{II}) of 88 cm^{-1}. This demonstrates stabilization of the grain side by excessive calcium carbonate, as compared with the deterioration of the flesh side. The above are clearly shown in the colorized spectra of Figure S4a–d. Besides, in the same figure, subtle envelope changes of the amide I band are also observed. Additionally, the amide II intensity decreases in

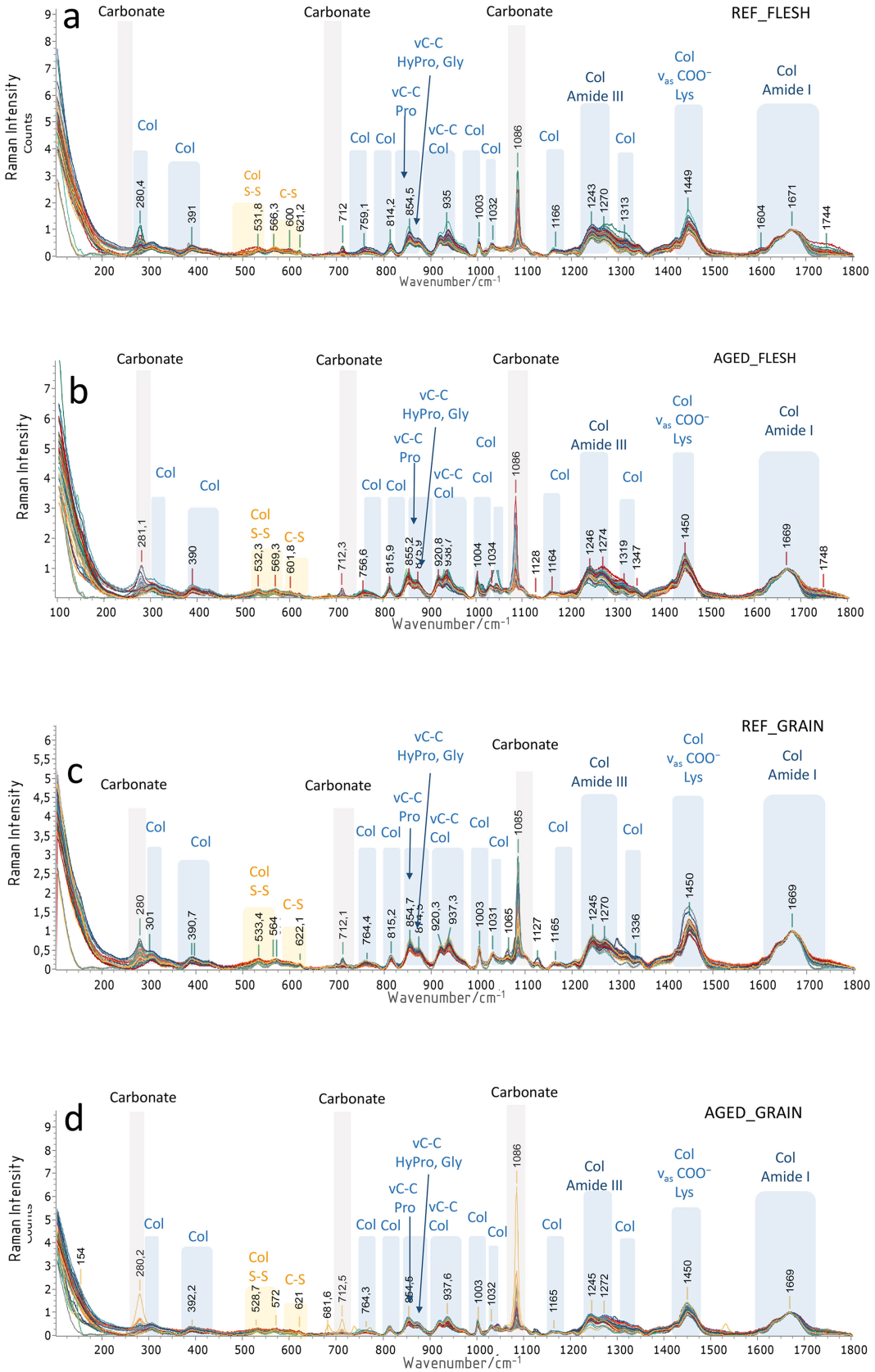

FIGURE 1 | Raman spectra of parchment samples: (a) flesh side, reference; (b) flesh side, aged; (c) grain side, reference; (d) grain side, aged. All spectra are normalized at the ~1670 cm^{-1} (amide I) band.

TABLE 2 | Raman spectroscopy bands and assignments of collagen-based materials.

Raman bands	Assignments[a]
1678 m	Amide I
1459 s	vas COO^-, Lysine
1429 vw	δNH3
1404 vw	vs COO^-, Lysine
1318 w	δNH
1275 sh	Amide III
1250 vs	Amide III
1171 wm	wCH_2, τNH_2, ρNH^{3+}, hydroxylysine
1102 sh	δNCH Pro
1031 vw	vC-N Pro
1002 m	Aromatic ring (Phenylalanine)
942 s	vC–C skeletal in Proline
925 sh	vC–COO^-
879 sh	vC–C in Glycine
859 m	vCC ring in Proline
822 m	vCC skeletal in aminoacids
763 wb	δNOO^-
622, 600 w	vC-S in cysteine/cystine and methionine residues
570	Aromatic in Phenylalanine
533 m	vS-S in cystine
397 vw	Skeletal deformation
305 vw	Skeletal deformation

Note: Assignments column: v, stretching; δ, bending; w, wagging; τ, twisting; ρ, rocking; i-p, in-plane; Raman Bands column: m, medium; s, strong; vw, very weak; w, weak; sh, shoulder; vs, very strong; wm, weak medium; wb, doublet.
[a]From [5, 27, 28, 56].

the cases with increasing carbonates, suggesting hydrolytic degradation. Finally, the carbonyl band at 1739 cm^{-1}, due to lipid ester groups, is highly variable in intensity and appears to be connected with the also intensity-variable carbonate bands.

4.3 | Second Derivative Spectra

Techniques such as band deconvolution and use of second derivative spectra have often been employed for the detailed analysis of broad infrared bands such as amide I and II [36, 64, 65]. The former has been quite successful in deconstructing the particular contributions in broadly enveloped bands [34, 63], offering a valuable assessment of the secondary and tertiary structures of proteins [36, 66, 67, 72]; however, it is time-consuming, especially in the case of high loads of spectrum data, such as in this particular work. Derivation of spectra, specifically resulting in the second derivative, has also been employed for broad infrared bands [8, 64, 66, 68–70]; the technique has the advantage of producing sharp bands from subtle inflection points of broad bands in original spectra, thus facilitating observation and evaluation of the various vibrational contributions, such as those in amide I and II protein bands. As mentioned above, the amide I and II bands show changes in their envelope and subtle shifts of local maxima. In Figure S3, two representative spectra are shown exemplifying these changes in the damaged protein of parchment (Curves 1 and 2, corresponding to healthy and damaged protein fractions, respectively); the corresponding second derivative spectra (1D and 2D) show sharp negative peaks which are deeper and left-shifted in curve 1D (1660, 1629, 1550, and 1519 cm^{-1}), as compared to 2D (respective minima at 1657, 1627, 1545, and 1508 cm^{-1}).

4.4 | Data Elaboration

The above observations justify the necessity for a chemometrics-based evaluation based on band maxima shift, intensity changes, and envelopes concerning aging conditions (see Section 2.3.3). As for comparison reasons, both Raman and FTIR spectra were normalized on amide I band (See Section 3.4); all intensity changes were considered against these maxima.

The only statistically important and intense (−0.445) correlation between the Raman and Infrared band intensities is the one for the 1245 cm^{-1} (Raman) with the 1230 cm^{-1} (FTIR). This negative correlation was unexpected, since this is a component of the amide III envelope active with both techniques. This result may be related either to an opposite effect of molecular symmetry on Raman shift and FTIR absorption, respectively [24, 63] or simply to the ambiguity caused by an overlap with other bands in the Raman spectra. Nonetheless, this interesting phenomenon merits further investigation.

Concerning the Raman bands, the following statistically significant correlations were detected. The strongest negative correlation was found in the NO_2-treated samples for peak intensities at 1002 cm^{-1} (phenylalanine ring stretch) and 1028 cm^{-1} (C–N stretch of Pro). Besides, the envelope of the broad amide I band at 1670 cm^{-1} was also found negatively correlated; this is confirmed by the corresponding correlation found for the FTIR amide I band (see below). Weaker correlations were found in the S/N order for the 1002 cm^{-1} band (positive), in the NO_2 treated samples for the 305 cm^{-1} band (negative), and in the SO_2 treated samples for the 622 cm^{-1} band (negative). For the vibrations involving S atoms, two significant correlations were confirmed: (a) in the SO_2 treated sample, a negative correlation for the 531 cm^{-1} band (i.e., the 531 cm^{-1} band intensity drops in the SO_2 treated samples) and (b) in the NO_2 treated sample, a positive correlation for the 570 cm^{-1} band (i.e., the 570 cm^{-1} band intensity increases in the NO_2 treated samples).

The reduction of the 531 cm^{-1} band intensity in the SO_2-treated samples points to its assignment as a ggg(-S-S-) disulfide bridge stretch, in analogy with an intensity reduction of a 510 cm^{-1} band observed for sheep parchment [5], which signals the reduction of the relatively weak disulfide bonds in the native protein with aging. The 570 cm^{-1} band intensity increase in the NO_2 treated samples is interesting, as it would be expected to increase in the SO_2 treated samples instead [5]; this is corroborated

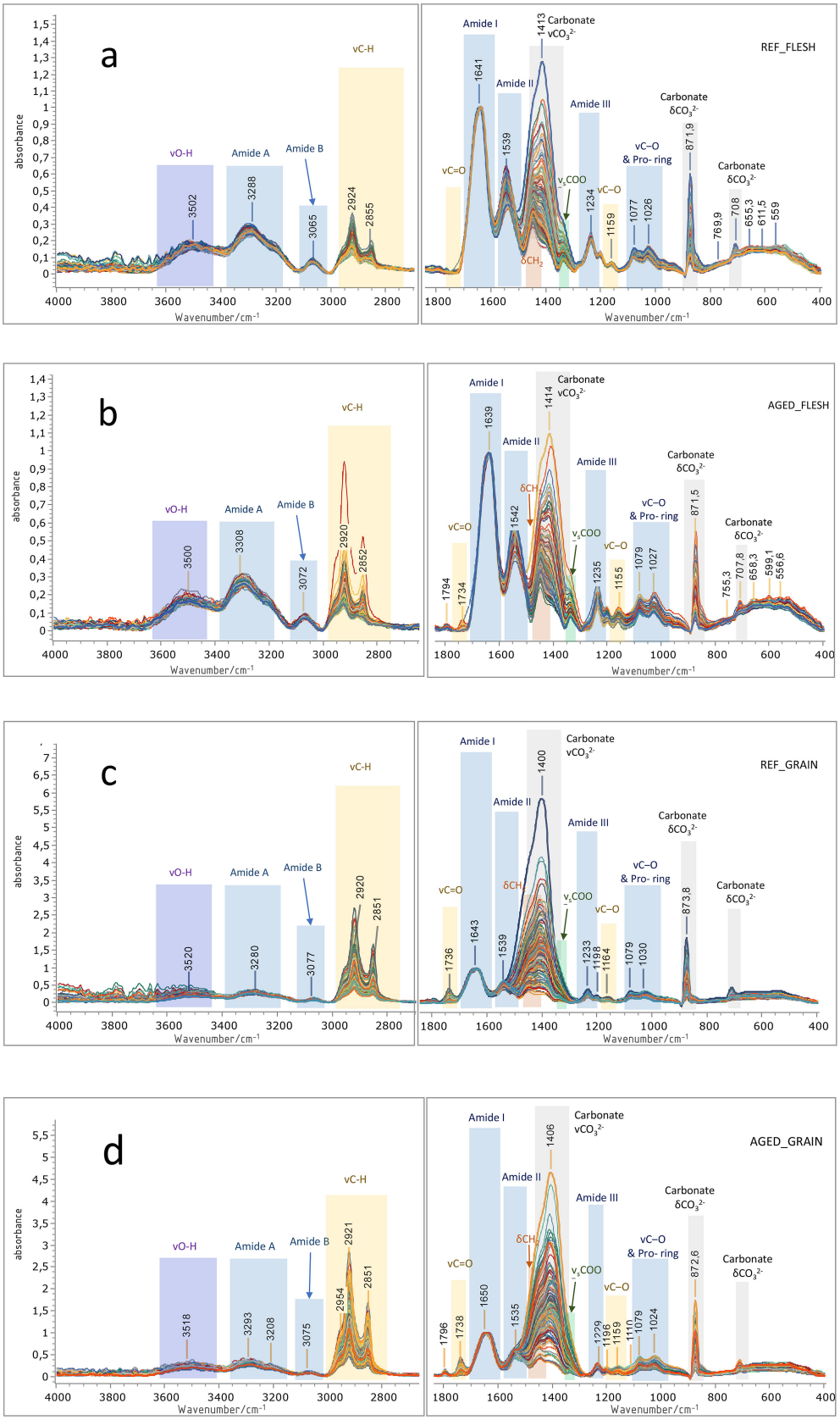

FIGURE 2 | FTIR spectra of parchment samples:s (a) flesh side, reference; (b) flesh side, aged; (c) grain side, reference; (d) grain side, aged. All spectra are normalized at the ~1650 cm^{-1} (amide I) band.

by the 1002 cm^{-1} observation, that is, affected by the S/N order. Based on its aromatic ring assignment (Table 2), it can be tentatively explained as a nitration effect of phenylalanine and/or tryptophan; substitution with groups conjugated to the aromatic ring (such as NO_2 groups) may increase aromatic ring vibration intensities [63].

TABLE 3 | Infrared bands and assignments.

Infrared band	Assignment[a]
3300–3100 (br)	Amide A: first component of vN-H Fermi resonance + amide I overtone
3072 (m-w)	Amide B: second component of vN-H Fermi resonance + amide II overtone
2920, 1850 (m)	vC-H (lipid fraction; glycine, proline units in protein fraction)
1739 (w)	vC=O (lipid fraction)
1644 (s)	Amide I: vC=O with minor contributions from vC-N and δN-H)
1538 (s)	Amide II: (vC-N with contributions from δ_{ip}N-H)
1448 (m)	δCH_2
1408 (w)	δ_{ip}C-O-H (carboxylic) and δNH_2 side chains
1334 (w)	wCH_2 + δC-H
1230, 1203 (m-w)	Amide III: (vC-N + δN-H with contributions from vC-C and δ_{ip}C=O)
1160	vC-O (lipid fraction)
1084 (w) 1031 (w)	vC-O lipids+breathing of proline ring; δi-pH-C-C in proline; glycosyl-sites in collagen

Note: Assignments column: v, stretching; δ, bending; w, wagging; τ, twisting; ρ, rocking; i-p, in-plane; Infrared Bands column: br:broad; m-w, medium-weak; m, medium; w, weak; s, strong.
[a]From [8, 34, 68–70].

At first approach, a correlation of FTIR bands was sought between the calcium carbonate peaks and selected bands of the organic component. Regarding the amide I and II bands, where the distance of their maxima is shorter in cases of low carbonate content, no specific correlation was found for aged samples as compared to the reference ones. On the other hand, the carbonyl band at 1739 cm^{-1} was found to be positively correlated to the carbonate maximum at 1430 cm^{-1}, which is expected as the grain side of most samples were fat-rich and also carried higher carbonate amounts. A correlation of 0.79 was found in the aged spectra as compared to 0.66 for the reference spectra, suggesting an intensified effect induced by aging. More particularly, the aging factor of NO_2 was found to have the most intense correlation with 0.85. This possibly suggests the selective location of calcium carbonate in lipid-rich spots.

Regarding the amide I band (envelope around its maximum at 1645–1625 cm^{-1}) of the original spectra, no significant correlation was found with any of the aging factors. On the other hand, the intensity of the amide II band (1520–1540 cm^{-1}) recorded in the flesh side of samples, a marker for hydrolytic degradation, was significantly correlated with humidity and SO_2, suggesting a detectable deterioration effect for parchment collagen under the specific aging conditions induced by acidic hydrolysis (i.e., the combination of sulfur oxides with humidity).

TABLE 4 | Associations regarding aging factors in statistically significant Raman and FTIR bands.

Assignment	Raman						FTIR				
	RAMAN mode	FTIR mode	Duration	Humidity	SO_2	NO_2	Order	Duration	Humidity	SO_2	NO_2	Order
Amide I	1670	1640				**						
Amide II		1540							**	**		
Amide III	1245	1230										
vC-N (Pro)	1028					**						
Aromatic stretch (Phe)	1002					**	*					
vC-S	622				*							
Aromatic Phe, Trp	570					*						
vS-S	531				*							
Skeletal	305					*						

TABLE 5 | Correlation between paired modes of RAMAN and FTIR.

RAMAN maxima (cm^{-1})	FTIR maxima (cm^{-1})	Significant at 5%
1670	1640	−0.050 (0.633)
1450	1550	0.021 (0.857)
1245	1230	−0.445 (<0.001)**
1085	1430	−0.082 (0.500)
710	712	−0.198 (0.100)
280	873	−0.239 (0.054)

Note: It has been used Pearson correlation coefficient using significance level 0.05.

The second derivative curves of the amide I and II bands (see example curves in Figure S3) showed a small positive correlation (0.05) of the amide II minima at 1583, and 1555 cm^{-1} with SO_2, humidity, while no significant correlation was found for 1665 cm^{-1} (amide I). "Positive correlation" suggests an increase of the long-wavenumbers inflection points of amide II, which corresponds to the onset of this band's upshifting that finally results in a decrease of the (amide I and amide II) maxima difference; this difference has been proposed as a criterion for parchment damage [35, 71].

As a result of the above, a minimal, albeit detectable effect of these specific aging conditions on collagen's secondary structure can be observed. This finding, in combination with the correlation found in the S–S Raman band (see above), may signify that S–S cleavage induced by SO_2-induced aging contributes to changes in the secondary structure of the protein [35, 71].

Concerning the influence of the sample position in the hide on the effect in the results, it is found that this is not the case [35, 71].

Table 4 presents the results from the ANOVA model with respect several modes of both Raman and FTIR spectrometry. The first column presents the name of the mode and what the mode is representing. The results for the modes of FTIR and Raman are presented separately. A "*" implies statistical significance on 5% confidence level, while "**" implies significance at 5% after Bonferroni correction for multiplicity to eliminate the case of false positive results.

Table 5 presents the results when matching the different modes of the different spectrometry methods was tried. Each pair corresponds to measuring the same vibrations. It has used Pearson correlation coefficient using significance level 0.05. We report the Pearson correlation value and the *p*-value in parenthesis. Only the pair 1245 (amide III in Raman) and 1230 cm^{-1} (amide III in FTIR) was found significantly different than zero (observed correlation = −0.44). The correlation coefficient was calculated from all the available sample (216 samples). For all the other modes rejection, the null hypothesis of zero correlation was failed, so what it was observed can be attributed to pure chance. The results bring forward an interesting point of complementarity since the two methods seem to behave differently even for matched modes.

The negative value for the most statistically significant maxima (i.e., the amide III band at 1245 and 1230 cm^{-1}) suggests an opposite, yet clear response for this vibration, possibly, due to the different effect of molecular symmetry on Raman shift and FTIR absorption, respectively [24, 63]. Nonetheless, this interesting phenomenon merits further investigation.

According to Larsen [6], the damage of collagen in parchment may occur at various levels such as the macrolevel, microlevel, and nanolevel, which may not be necessarily observable through standard analytical investigative means at all levels simultaneously. Therefore, it appears obvious that the onset of changes needs to be further combined and eventually complemented with other analytical techniques, such as thermal techniques. Coupling of the measurements obtained through this work with shrinking temperature investigations through micro-hot table analysis, which has been previously shown to provide a significant insight of the overall damage of collagen fibers within parchment [6], may provide a better understanding for the onset of changes induced under mild conditions so that possible damaging conditions be signaled and warned by conservators.

5 | Conclusions

The main objective of this research was to examine the impact of mild environmental conditions on the structural and material integrity of artificially aged goat parchment samples. For the first time, statistics have been used in advance to organize the experimental design of artificial aging of parchment to determine its degradation in early stages. Raman and FTIR analyses were used to investigate the degradation at the molecular level.

Advanced statistical data elaboration was applied on data from Raman and FTIR spectra in correlation with artificial aging (exposure of samples cut from a single goat skin to sulfur and nitrogen oxides at concentrations similar to those in a typically polluted urban atmosphere, at constant room temperature, two different time periods, and two different moisture levels) of parchment to determine its degradation.

To further substantiate the Raman and FTIR observations despite their subtlety, statistical treatment of the entire spectra data through ANOVA was carried out, which showed correlations of Raman and FTIR bands with specific aging conditions at some level. A correlation was found between humidity and

sulfur oxides with hydrolytic damage as reflected by changes in amide I, II, and III bands in the spectra, suggesting acidic hydrolysis. More specifically, the envelope of the amide I Raman band was negatively correlated with (namely found to be narrower in) NO_2-treated samples, suggesting that changes are induced by nitrogen oxides in the secondary and tertiary structures of collagen; however, this was not confirmed through a clear correlation of the corresponding FTIR bands. On the other hand, the amide II band, more clearly seen in the FTIR spectra of flesh side, is found to be affected by humidity and sulfur oxides, which, combined, are responsible for hydrolytic degradation, also affecting the secondary and tertiary structures of the protein. A similar result was also obtained by considering the trend of other bands, such as the S–S disulfide Raman band, which is negatively correlated with sulfur oxides (i.e., decreased with high SO_2 concentrations). Finally, the amide III bands shown in both Raman and FTIR were negatively correlated between themselves, a result that merits further investigation of molecular symmetry considerations in the two techniques.

In all cases, weakly or minimally statistically significant trends were detected, as the result of the mild aging conditions, that is, low concentrations of sulfur and nitrogen oxides, which were selected for this work. These conditions (as opposed to conditions typically adopted for accelerated aging experiments, reported elsewhere) were designed to monitor the onset of chemical changes in the parchment material as recorded in the spectra. The statistical significance of the observed correlations allows us to mark small changes in Raman and FTIR bands, which are typically overlooked, as the beginning of alterations, which may assist the conservator to take precautions on parchment objects before more significant damage occurs.

The simulation of organic materials' natural aging is a very complicated task due to the multifactorial character of this process. At this point, we demonstrate that the contribution of statistics to analytical research procedures may help disclose and highlight hidden information within analytical results.

Furthermore, given that the two methods highlight different vibrational aspects of the bonding within the same material, a complementarity is being demonstrated regarding the information they offer for aging-induced changes either on the vibrations of identical bonds or on structural changes depending on different bonding which correspondingly highlight different aspects of molecular changes.

In conclusion, the combination of Raman spectroscopy and FTIR can provide remarkable data on the investigation of parchment degradation. Their complementarity alongside other analytical techniques may result in the interpretation of analytical data in the framework of chemometric methods.

Acknowledgments

The authors are grateful to Prof. Georgios Panagiaris (Department Conservation of Antiquities & Works of Art, University of West Attica) for the thorough discussions, insightful comments, and continuous support throughout this research and the formulation of this paper; to Vasileios Krithiotis, Conservator of Archival Materials, for his technical support in the preparation of the samples; and to Roza Papoutsaki-Rapti, Yannis Tzanakis, Crhistrina Sakellariou, and to Assoc. Prof. Dimitrios Makris for the assistance in matters of data illustration. The publication of the article in OA mode was financially supported by HEAL-Link.

Conflicts of Interest

The authors declare no conflicts of interest.

References

1. Liszewska W., "New Methods of Leafcasting in the Conservation of Historic Parchments, Polish Institute of World Art Studies," Academy of Fine Arts in Warsaw, Warsaw, (2017).

2. M. Chapuis, A. Lydon, and A. Brandt-Grau, *Preserving our Heritage, Improving Our Environment. Volume II, Cultural Heritage Research* (Luxenbourg: Publications Office Of The European Union, 2009).

3. R. Larsen, D. V Poulsen, F. Juchauld, et al., "In 14th Triennial Meeting, The Hague, 12–16 September 2005: Preprints (Icom Committee For Conservation)," (2005).

4. F. Juchauld, H. Jerosch, K. Dif, R. Ceccarelli, S. Thao, "Improved Damage Assessment of Parchment. I.D.A.P. Assessment, Effects of Two Pollutants (so2 and no2) on Parchment by Analysis at the Molecular Level Using Mass Spectrometry and Other Techniques," Correlation With Differential Scanning Calorimetry and Visu, (2007).

5. A. Malissa, F. Cappa, M. Schreiner, and M. Marchetti-Deschmann, "Spectral Features Differentiate Aging-Induced Changes in Parchment—A Combined Approach of UV/VIS, μ-ATR/FTIR and μ-Raman Spectroscopy With Multivariate Data Analysis," *Molecules* 28, no. 12 (2023): 4584, https://doi.org/10.3390/molecules28124584.

6. R. Larsen, "Improved Damage Assessment of Parchment," I.D.A.P. Assessment, Data Collection and Sharing of Knowledge, (2007).

7. M. Vest, J. Jacobsen, R. Larsen, "Improved Damage Assessment of Parchment," I.D.A.P. Assessment, accelerated ageing effect of heat and relative humidity, (2007).

8. M. Odlyha, C. Theodorakopoulos, J. De Groot, L. Bozec, and M. Horton, "Fourier Transform Infra-red Spectroscopy (ATR/FTIR) and Scanning Probe Microscopy of Parchment," *E-Preservation Science* 6 (2009): 138–144.

9. P. Budrugeac, E. Badea, G. Della Gatta, L. Miu, and A. Comănescu, "A DSC Study of Deterioration Caused by Environmental Chemical Pollutants to Parchment, a Collagen-Based Material," *Thermochimica Acta* 500 (2010): 51–62.

10. M. Ciglanská, V. Jančovičová, B. Havlínová, Z. Machatová, and V. Brezová, "The Influence of Pollutants on Accelerated Ageing of Parchment With Iron Gall Inks," *Journal of Cultural Heritage* 15 (2014): 373–381.

11. M. S. Kern, A. Pataki-Hundt, J. Wouters, and D. P. Kirby, "Accelerated Ageing of Parchment: Investigation of a Photo Catalysed, Low-Heat Approach," *Restaurator-International Journal for the Preservation of Library and Archival Material* 13 (2018): 15.

12. C. Cicero, F. Mercuri, S. Paoloni, et al., "Integrated Adiabatic Scanning Calorimetry, Light Transmission and Imaging Analysis of Collagen Deterioration in Parchment," *Thermochimica Acta* 676 (2019): 263–270, https://doi.org/10.1016/j.tca.2019.05.007.

13. F. Cappa, I. Paganoni, C. Carsote, M. Schreiner, and E. Badea, "Studies on the Effect of dry-Heat Ageing on Parchment Deterioration by Vibrational Spectroscopy and Micro Hot Table Method," *Polymer Degradation and Stability* 182 (2020): 1.

14. C. J. Kennedy and T. J. Wess, "The Structure of Collagen Within Parchment – A Review," *Restaurator* 24 (2003): 61.

15. R. Reed, "Ancient Skins, Parchments and Leathers, London," (1972).

16. M. Fourneau, C. Canon, D. Van vlaender, et al., "Histological Study of Sheep Skin Transformation During the Recreation of Historical Parchment Manufacture," *Heritage Science* 8 (2020): 1.

17. T. J. Wess, "Collagen Fibril Form and Function," *Advances in Protein Chemistry* 70 (2005): 341.

18. D. V. P. Sommer and R. Larsen, "Detection of COL III in Parchment by Amino Acid Analysis," *Amino Acids* 48 (2016): 169–181.

19. L. Bozec, G. Van der Heijden, and M. Horton, "Collagen Fibrils: Nanoscale Ropes," *Biophysical Journal* 92 (2007): 70–75.

20. E. Heidemann, "Fundamentals of Leather Manufacture, Eduard Roether kg, Darmstadt," (1993).

21. P. R. Griffiths and J. A. De Haseth, *Fourier Transform Infrared Spectrometry*, second ed. (Hoboken, New Jersey: John Wiley & Sons, 2006).

22. P. R. Griffiths, *Handbook of Vibrational Spectroscopy* (chichester: John Wiley & Sons, Ltd, 2010).

23. M. Jackson and H. H. Mantsch, *Handbook of Vibrational Spectroscopy* (chichester: John Wiley & Sons, Ltd, 2006).

24. H. G. M. Edwards and J. M. Chalmers, *Raman Spectroscopy in Archaeology and art History* (london: The Royal Society Of Chemistry, 2005).

25. P. Vandenabeele and H. G. M. Edwards, *Raman Spectroscopy in Archaeology and Art History*, vol. 2 (Cambridge: The Royal Society Of Chemistry, 2019).

26. S. Rangan, H. G. Schulze, M. Z. Vardaki, M. W. Blades, J. M. Piret, and R. F. B. Turner, "Applications of Raman Spectroscopy in the Development of Cell Therapies: State of the Art and Future Perspectives," *Analyst* 145 (2020): 2070–2105.

27. H. G. M. Edwards, D. W. Farwell, E. M. Newton, F. Rull perez, and S. J. Villar, "Application of FT-Raman Spectroscopy to the Characterisation of Parchment and Vellum, I; Novel Information for Paleographic and Historiated Manuscript Studies," *Spectrochimica Acta Part A: Molecular and Biomolecular Spectroscopy* 57 (2001): 1223–1234.

28. H. G. M. Edwards and F. R. Perez, "Application of Fourier Transform Raman Spectroscopy to the Characterization of Parchment and Vellum. II—Effect of Biodeterioration and Chemical Deterioration on Spectral Interpretation," *Journal of Raman Specroscopy* 35 (2004): 754–760.

29. M. N. Dole, P. A. Patel, and S. D. Sawant, "Advance Applications of Fourier Transform Infrared Spectroscopy," *International Journal of Pharmaceutical Sciences Review and Research* 7, no. 2 (2011): 159–166.

30. T. Buffeteau, B. Desbat, and D. Eyquem, "Attenuated Total Reflection Fourier Transform Infrared Microspectroscopy: Theory and Application to Polymer Samples," *Vibrational Spectroscopy* 11 (1996): 29–36.

31. R. Schütz, l. Bertinetti, I. Rabin, P. Fratzl, and A. Masic, "Quantifying Degradation of Collagen in Ancient Manuscripts: The Case of the Dead sea Temple Scroll," *Analyst* 138 (2013): 5594–5599.

32. M. Bicchieri, M. Monti, G. Piantanida, F. Pinzari, and A. Sodo, "Non-destructive Spectroscopic Characterization of Parchment Documents," *Vibrational Spectroscopy* 55 (2011): 267–272.

33. A. Možir, M. Strlič, T. Trafela, et al., "On Oxidative Degradation of Parchment and Its Non-Destructive Characterisation and Dating," *Applied Physics a: Materials Science & Processing* 104 (2011): 211–217.

34. S. C. Boyatzis, G. Velivasaki, and E. Malea, "A Study of the Deterioration of Aged Parchment Marked With Laboratory Iron Gall Inks Using FTIR-ATR Spectroscopy and Micro Hot Table," *Heritage Science* 4 (2016): 1.

35. G. Vyskočilová, M. Ebersbach, R. Kopecká, L. Prokeš, and J. Příhoda, "Model Study of the Leather Degradation by Oxidation and Hydrolysis," *Heritage Science* 7 (2019): 1.

36. A. Barth and C. Zscherp, "What Vibrations Tell About Proteins," *Quarterly Reviews of Biophysics* 35 (2002): 369–430.

37. A. Barth, "The Infrared Absorption of Amino Acid Side Chains," *Progress in Biophysics and Molecular Biology* 74 (2000): 141–173.

38. T. Riaz, R. Zeeshan, F. Zarif, et al., "Ftir Analysis of Natural and Synthetic Collagen," *Applied Spectroscopy Reviews* 53 (2018): 703–746.

39. M. A. Bryan, J. W. Brauner, G. Anderle, C. R. Flach, B. Brodsky, and R. Mendelsohn, "Ftir Studies of Collagen Model Peptides: Complementary Experimental and Simulation Approaches to Conformation and Unfolding," *Journal of the American Chemical Society* 129 (2007): 7877–7884.

40. S. C. Boyatzis, *Materials in Art and Archaeology Through Their Infrared Spectra* (New York: Nova Science Publishers, 2022).

41. X. Zou, T. Uesaka, and N. Gurnagul, "Prediction of Paper Permanence by Accelerated Aging I. Kinetic Analysis of the Aging Process," *Cellulose* 3 (1996): 243–267.

42. R. Larsen, D. S. P. Vestergaard, M. Odlyha, et al., *Microanalysis of Parchment* (London: Archetype Publications Ltd, 2002).

43. D. J. Bechmann, R. Larsen, "Improved Damage Assessment of Parchment. I.D.A.P. Assessment, Data Collection and Sharing of Knowledge," (2007).

44. S. Zervos, "Restaurator," https://doi.org/10.1515/rest.2007.256.

45. D. C. Deselnicu, "Leather Footwear J," (2010): 10–13.

46. E. Malea, E. Papageorgiou, G. Panagiaris, "Int. Conf. Integr. Inf. (ic-ininfo 2011)."

47. S. Zervos, "In Cellulose: Structure And Properties, Derivatives and Industrial Uses," (2010).

48. E. Malea, T. Vogiatzi, D. E. Watkinson, "In Proceedings of the 11th ICOM-CC Group on Wet Organic Archaeological Materials Conference, Greenville 2010," (2012).

49. P. Dellaportas, E. Papageorgiou, and G. Panagiaris, "Museum Factors Affecting the Ageing Process of Organic Materials: Review on Experimental Designs and the Invenvorg Project as a Pilot Study," *Heritage Science* 2 (2014): 1.

50. G. Thomson, *The Museum Environment, Butterworth*, 2nd ed. (london: Heinemann, 1986).

51. Y. Kobayashi and K. Yoshizumi, "Soiling and Deterioration of Wool Fiber due to Exposure to Atomspheric Environment," *Environmental Sciences* 50 (1994): 402–405.

52. O. J. Dunn, "Multiple Comparisons Among Means," *Journal of the American Statistical Association* 56 (1961): 52–64.

53. G. E. P. Box, J. S. Hunter, and W. G. Hunter, *Statistics of Experimenters Design, Innovation, and Discovery*, 2nd ed. (Hoboken, New Jersey: John Wiley & Sons, Inc., 2005).

54. D. C. Montgomery, *Design and Analysis of Experiments*, 8th ed. (Hoboken, New Jersey: John Wiley & Sons, Incorporated, 2012).

55. S. H. Urashima, T. Nishioka, and H. Yui, "Micro-Raman Spectroscopic Analysis on Natural Carbonates: Linear Relations Found via Biaxial Plotting of Peak Frequencies for Cation Substituted Species," *Analytical Sciences* 38 (2022): 921–929.

56. C. R. Flach and D. J. Moore, "Infrared and Raman Imaging Spectroscopy of Ex Vivo Skin," *International Journal of Cosmetic Science* 35 (2013): 125–135.

57. A. S. Dichiara, R. C. Li, P. H. Suen, et al., "A Cysteine-Based Molecular Code Informs Collagen C-Propeptide Assembly," *Nature Communications* 9, no. 1 (2018): 4206, https://doi.org/10.1038/s41467-018-06185-2.

58. D. Barth, H. J. Musiol, M. Schütt, et al., "The Role of Cystine Knots in Collagen Folding and Stability, Part I. Conformational Properties of

(Pro-Hyp-Gly) 5 and (Pro-(4S)-FPro-Gly) 5 Model Trimers With an Artificial Cystine Knot," *Chemistry a European Journal* 9 (2003): 3692–3702.

59. D. Barth, O. Kyrieleis, S. Frank, C. Renner, and L. Moroder, "The Role of Cystine Knots in Collagen Folding and Stability, Part II. Conformational Properties of (Pro-hyp-gly)nmodel Trimers With n- and c-Terminal Collagen Type III Cystine Knots," *Chemistry a European Journal* 9 (2003): 3703–3714.

60. N. Prieto-Taboada, A. Larrañaga, O. Gómez-Laserna, and I. Martínez-Arkarazo, "The Relevance of the Combination of xrd and Raman Spectroscopy for the Characterization of the caso4–h2o System Compounds," *Microchemical Journal* 122 (2015): 102–109.

61. M. H. Brooker, "Raman and ir Spectra of Zinc, Cadmium and Calcium Nitrate: A Study of the Low Temperature Phase Transitions in Calcium Nitrate," *Spectrochimica Acta Part A: Molecular Spectroscopy* 32 (1976): 369–377.

62. F. Zapata and C. García-ruiz, "The Discrimination of 72 Nitrate, Chlorate and Perchlorate Salts Using IR and Raman Spectroscopy," *Spectrochimica Acta Part A: Molecular and Biomolecular Spectroscopy* 189 (2018): 535–542.

63. D. Mayo, F. Miller, and R. Hannah, *Course Notes on the Interpretation of Infrared and Raman Spectra* (New Jersey: Wiley, 2004).

64. J. Bandekar and S. Krimm, "Vibrational Analysis of Peptides, Polypeptides, and Proteins: Characteristic Amide Bands of B-Turns," *Proceedings of the National Academy of Sciences of the United States of America* 76 (1979): 774–777.

65. S. Krimm and J. Bandekar, "Vibrational Analysis of Peptides, Polypeptides, and Proteins. V. Normal Vibrations of β-Turns," *Biopolymers: Original Research on Biomolecules* 19, no. 1 (1980): 1–29.

66. G. W. Lucassen, "Band Analysis of Hydrated Human Skin Stratum Corneum Attenuated Total Reflectance Fourier Transform Infrared Spectra in Vivo," *Journal of Biomedical Optics* 3 (1998): 267–280.

67. M. M. Borah, "Structural and Spectroscopic Analysis OFL-Prolinemonomer and Dimer Bydftapproach," *Vietnam Journal of Chemistry* 60 (2022): 718–737.

68. E. Mannucci, R. Pastorelli, G. Zerbi, C. Bottani, and A. Facchini, "Recovery of Ancient Parchment: Characterization by Vibrational Spectroscopy," *Journal of Raman Specroscopy* 31 (2000): 1089–1097.

69. F. Mallamace, P. Baglioni, C. Corsaro, et al., "The Influence of Water on Protein Properties," *Journal of Chemical Physics* 141, no. 16 (2014): 165104, https://doi.org/10.1063/1.4900500.

70. M. Bicchieri, M. Monti, G. Piantanida, et al., "Proc. Art2008 9th int. Conf. Jerusalem, ISR. May 25th–30th, Publ. On-line Database j. Non-Destructive Testing,{\Copyright} ndt," Net (2008), 25.

71. E. Badea, L. Miu, P. Budrugeac, et al., "Study of Deterioration of Historical Parchments by Various Thermal Analysis Techniques Complemented by SEM, FTIR, UV-Vis-NIR and Unilateral NMR Investigations," *Journal of Thermal Analysis and Calorimetry* 91 (2008): 17–27.

72. M. Sheena, L. Ushakumari, B. Harikumar, H. T. Varghese, and C. Y. Panicker, "FT-IR, FT-Raman and Sers Spectra of l-Proline," *Journal of the Iranian Chemical Society* 6 (2009): 138–144.

Supporting Information

Additional supporting information can be found online in the Supporting Information section.